Fermions and bosons : excitons in strongly correlated materials

Rademaker, L.

4
Exciton-spin dynamics in the Mott insulating state

Two fermions form a boson, which is precisely what happens when an electron and a hole bind together into an exciton. A completely different way to find emergent bosonic physics is to have strong electron-electron interactions near half-filling. In the Mott insulating state, the effective degrees of freedom are bosonic spin waves.

Whenever the electron-electron and electron-hole interactions are strong, which we expect in the case of cuprates, we can model the system in terms of bosons only: spins and excitons. In this chapter we derive the corresponding **exciton $t-J$ model**. Close to the Mott insulating state the insertion of excitons leads to frustration, as is described in section 4.2. The full phase diagram of the exciton $t-J$ model is discussed in the next chapter.

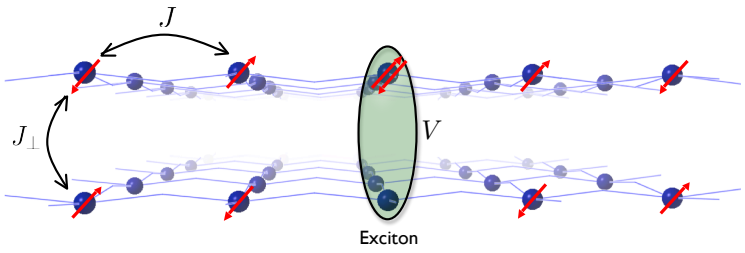

Figure 4.1: Naive real space picture of an exciton in a strongly correlated bilayer, as viewed from the side. Two square lattices (blue balls) are placed on top of each other. The red arrows denote the spin ordering, which forms a perfect Néel state. The exciton consists of a bound pair of a double occupied and a vacant site on an interlayer rung. The energy required to break this doublon-holon pair is V. The magnetic ordering is governed by the in-plane Heisenberg J and the interlayer $J_\perp$, as described by the Hamiltonian (4.12).

4.1 *Strong coupling limit and the $t-J$ model*

When the onsite Coulomb repulsion in the Hubbard model (3.4) is much larger than the kinetic energy, $U \gg t$, it becomes impossible for two electrons to occupy the same orbital. At half-filling this

results in a traffic jam of electrons: on each lattice site there is one electron, unable to move due to the restraint on double occupancy. This is the **Mott insulator**.[1]

[1] Mott, 1949; Anderson, 1952; and Marshall, 1955

4.1.1 *The Mott insulating state and the $t - J$ model*

The Mott insulating phase is thus characterized by a large interaction U and the corresponding localization of electrons at half-filling.[2] Due to this localization only the spin degree of freedom remains. A perturbation method by Kato, 1949 has been applied to the Hubbard model[3] to obtain an effective low energy model for the spins: the $t - J$ model.

[2] This is in stark contrast with the band theory picture, where electrons are completely delocalized.

[3] Klein and Seitz, 1973; Takahashi, 1977; and Chao et al., 1977

The key to this **strong coupling perturbation theory** is that we project out the states that contain double occupied sites.[4] The hopping terms H_t are treated as a perturbation on the exactly solvable interaction term H_U,

[4] On the electron doped side of half-filling we project out states with more double occupied sites than necessary, which is equivalent to projecting out the empty sites.

$$H_\lambda = H_U + \lambda H_t. \tag{4.1}$$

We introduce a projection operator $\mathbf{P}_0$ that projects onto the eigenspace U_0 of H_U with eigenvalue E_0 associated with a fixed number of double occupied sites. The hopping term is then adiabatically turned on, that is $\lambda \to 1$. Introduce an operator $\mathbf{P}_\lambda$ that projects onto the eigenspace U that is adiabatically connected to the eigenspace U_0. This operator is expressed in terms a contour integral over the resolvent operator,

$$\mathbf{P}_\lambda = \frac{1}{2\pi i} \oint_C \frac{dz}{z - H_\lambda} \tag{4.2}$$

where the contour C goes around the eigenvalue E_0 but not around any other eigenvalues of H_U. A series expansion of the resolvent operator yields

$$\mathbf{P}_\lambda = \mathbf{P}_0 + \lambda \left[\mathbf{P}_0 H_t \left(\frac{1 - \mathbf{P}_0}{E_0 - H_U} \right) + \left(\frac{1 - \mathbf{P}_0}{E_0 - H_U} \right) H_t \mathbf{P}_0 \right] + \mathcal{O}(\lambda^2). \tag{4.3}$$

Now an effective Hamiltonian on the eigenspace U exists, with exactly the same spectrum as the full H_λ, given by

$$H_{\text{eff}} = \mathbf{P}_0 (H_\lambda - E_0) \mathbf{P}_\lambda \mathbf{P}_0, \tag{4.4}$$

which can be constructed using the expansion of $\mathbf{P}_\lambda$. At zeroth order in λ the effective Hamiltonian consists of the electron hopping

term with the no double occupancy constraint,

$$H_{\text{eff}}^{(0)} = \mathbf{P}_0 H_t \mathbf{P}_0. \tag{4.5}$$

From now on the projection $\mathbf{P}_0$ is included as implicit constraint on the double occupancy.

The first order correction in λ is given by

$$H_{\text{eff}}^{(1)} = -\frac{1}{U}\mathbf{P}_0 H_t (1-\mathbf{P}_0) H_t \mathbf{P}_0. \tag{4.6}$$

It contains two-hopping processes, where the intermediate state contains an additional double occupied state as shown in table 4.1. The remaining Hamiltonian can be expressed in **spin operators** only, which are

$$s_i^z = \frac{1}{2}\left(c_{i\uparrow}^\dagger c_{i\uparrow} - c_{i\downarrow}^\dagger c_{i\downarrow}\right), \tag{4.7}$$

$$s_i^+ = c_{i\uparrow}^\dagger c_{i\downarrow}, \tag{4.8}$$

$$s_i^- = c_{i\downarrow}^\dagger c_{i\uparrow}. \tag{4.9}$$

Since the virtual exchange processes can only occur when neighboring spins are opposite, the Hamiltonian now equals the **antiferromagnetic Heisenberg model** with $J = \frac{t^2}{4U}$,

$$H_{\text{eff}}^{(1)} = J \sum_{\langle ij \rangle} \mathbf{s}_i \cdot \mathbf{s}_j. \tag{4.10}$$

The hopping term (4.5) together with the superexchange term (4.10) form the famous $t-J$ **model**.[5] It is a low-energy description of the Hubbard model close to half-filling and in the limit of large U. Note that now the concept of doping near this Mott insulating state has a different meaning than in standard semiconductors. The addition of electrons, known as electron-doping or n-doping, leads to extra double occupied sites which are called **doublons**. Similarly the removal of an electron (hole-doping or p-doping) introduces vacant sites which are called **holons**.

[5] Strictly speaking, the perturbation series at first order in λ also contains a density-density interaction and a three-site hopping process. Those are usually neglected (Imada et al., 1998).

Table 4.1: The first order in λ processes in the strong coupling perturbation series for the Mott insulating state, given by $\mathbf{P}_0 H_t (1-\mathbf{P}_0) H_t \mathbf{P}_0$. The initial and final states cannot have double occupied sites.

Initial state	Intermediate states (with double occupied site)	Final states	Process (in units of t^2)	
$\cdots \uparrow_i \downarrow_j \cdots$	$\cdots \uparrow\downarrow_i\, o_j \cdots$	$\cdots \uparrow_i \downarrow_j \cdots$	$2\hat{n}_{i\sigma}\hat{n}_{j\overline{\sigma}}$	$= -4s_i^z s_j^z + 1$
	$\cdots o_i \uparrow\downarrow_j \cdots$	$\cdots \downarrow_i \uparrow_j \cdots$	$2\hat{c}_{j\overline{\sigma}}^\dagger \hat{c}_{i\overline{\sigma}} \hat{c}_{i\sigma}^\dagger \hat{c}_{j\sigma}$	$= -2s_i^\pm s_j^\mp$

4.1.2 *The p- and n-doped bilayer*

Heterostructures of p- and n-doped cuprates can be typically described by a **bilayer $t-J$ model**: two single-layer $t-J$ models together with interlayer interactions. The hopping of electrons in each layer is given by

$$H_t = -t_e \sum_{\langle ij\rangle\sigma\ell} c^\dagger_{i\ell\sigma} c_{j\ell\sigma} + h.c. \tag{4.11}$$

with the double occupancy constraint left implicit. The undoped Mott insulating state is described by the bilayer Heisenberg model

$$H_J = J \sum_{\langle ij\rangle\ell} \mathbf{s}_{i\ell} \cdot \mathbf{s}_{j\ell} + J_\perp \sum_i \mathbf{s}_{i1} \cdot \mathbf{s}_{i2}. \tag{4.12}$$

Here $c^\dagger_{il\sigma}$ and $\mathbf{s}_{il}$ denote the electron and spin operators respectively on site i in layer $l = 1, 2$. The Heisenberg H_J is antiferromagnetic with $J > 0$ and $0 < J_\perp < J$.

Additionally we need to include the interlayer Coulomb attraction between a vacant site (holon) and double-occupied site (doublon) on the same rung, described by

$$H_V = V \sum_i n_{i1} n_{i2}. \tag{4.13}$$

This is the force that binds interlayer excitons. Without loss of generality, we assume that layer '1' contains the excess electrons with the constraint $\sum_\sigma c^\dagger_{i1\sigma} c_{i1\sigma} \geq 1$ and layer '2' has the constraint $\sum_\sigma c^\dagger_{i2\sigma} c_{i2\sigma} \leq 1$. In other words: we have n- and p-type doping in layer '1' and '2', respectively.

The full **bilayer $t-J$ model**

$$H_{bt-J} = H_t + H_J + H_V \tag{4.14}$$

is the large U limit of the extended bilayer Hubbard model (3.7). Understanding the **bilayer Heisenberg model** (4.12) will be an important step towards analyzing physics of a p/n-doped bilayer.

The bilayer Heisenberg Hamiltonian has been studied quite extensively using Quantum Monte Carlo (QMC) methods,[6] dimer expansions[7] and the closely related bond operator theory,[8] the nonlinear sigma model[9] and spin wave theory.[10] All results indicate a O(3) quantum nonlinear sigma model universality class quantum phase transition at a critical value of $J_\perp/J$ from an antiferromagnetically ordered to a disordered state, see figure 4.2. A

[6] Sandvik et al., 1995; and Sandvik and Scalapino, 1994

[7] Weihong, 1997; Gelfand, 1996; and Hida, 1992

[8] Matsushita et al., 1999; and Yu et al., 1999

[9] van Duin and Zaanen, 1997; and Chakravarty et al., 1989

[10] Miyazaki et al., 1996; Millis and Monien, 1993; Matsuda and Hida, 1990; and Hida, 1990

naive mean field picture of the antiferromagnetic ground state is provided by the Néel state, in which each of the sublattices are occupied by either spin up or spin down electrons as shown in figure 4.1. However, the exact ground state is scrambled by spin flip interactions reducing the Néel order parameter to about 60% of its mean field value.[11] A finite interlayer coupling $J_\perp$ generically reduces the antiferromagnetic order further. In the limit of infinite $J_\perp$, the electrons will form a valence bond solid of pair-singlets living on the interlayer rungs, destroying the antiferromagnetic order.

[11] Manousakis, 1991

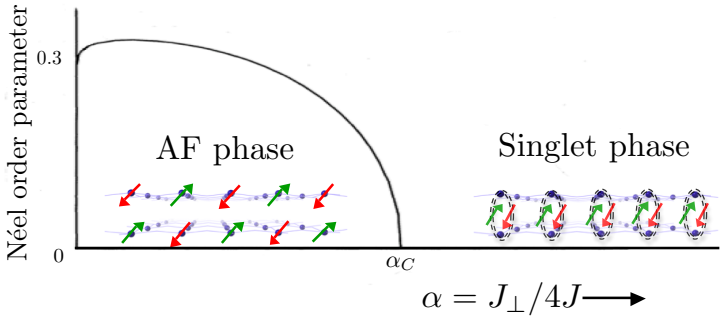

Figure 4.2: Zero temperature phase diagram of the bilayer Heisenberg model as a function of interlayer coupling strength $\alpha = \frac{J_\perp}{4J}$ on the horizontal axis. At a critical value α_c a quantum phase transition exists from the antiferromagnetic to the singlet phase. The vertical axis shows the Néel order parameter signaling antiferromagnetism. Note that even at $\alpha = 0$ the Néel order parameter is reduced from the mean field value $\frac{1}{2}$ to approximately 0.3 due to spin flip interactions. (Adapted from Chubukov and Morr, 1995.)

Standard linear spin wave theories cannot quite account for the critical value of $J_\perp/J \sim 2.5$ found in QMC and series expansion studies. This discrepancy between numerical results and the spin wave theory has a physical origin. Chubukov and Morr, 1995 pointed out that standard spin wave theories do not take into account the longitudinal (that is, the interlayer) spin modes. By incorporating such longitudinal spin waves one can derive analytically the right phase diagram.[12]Another correct method is to introduce an auxiliary interaction which takes care of the hard-core constraint on the spin modes.[13]

[12] Sommer et al., 2001

[13] Kotov et al., 1998

If one wants to study the doped bilayer antiferromagnet however, one needs explicit expressions of how a moving **dopant** (be it a hole, electron or exciton) **interacts with the spin excitations**. Even though the Néel state is just an approximation to the antiferromagnetic ground state, it provides an intuitive explanation for the major role spins play in the dynamics of any dopant. As can be seen in figure 4.3, a moving exciton causes a mismatch in the previously perfect Néel state. Consequently, the motion of an

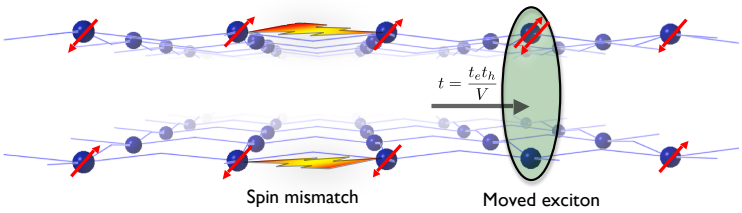

Figure 4.3: Exciton motion in a naive real space picture. In a perfect Néel state, the motion of an exciton (with respect to the situation in figure 4.1) causes a mismatch in the spin ordering. The kinetic energy gained by moving the exciton is proportional to the energies of the doublon t_e and holon t_h divided by the exciton binding energy V.

exciton is greatly hindered and a full understanding of possible spin wave interactions is needed to describe the exciton dynamics. This is of course similar to the motion of a single hole in a single Mott insulator layer.[14] It is also similar to the works of Vojta and Becker, 1999, who have computed the spectral function of a single hole in the Heisenberg bilayer. Therefore a rung linear spin wave approximation[15] is needed to obtain the expressions for the spin waves in terms of single site spin operators. Let us, however, first focus on the exciton properties of the p/n-doped bilayer.

[14] Schmitt-Rink et al., 1988; and Kane et al., 1989

[15] Sommer et al., 2001

4.1.3 *The exciton $t - J$ model*

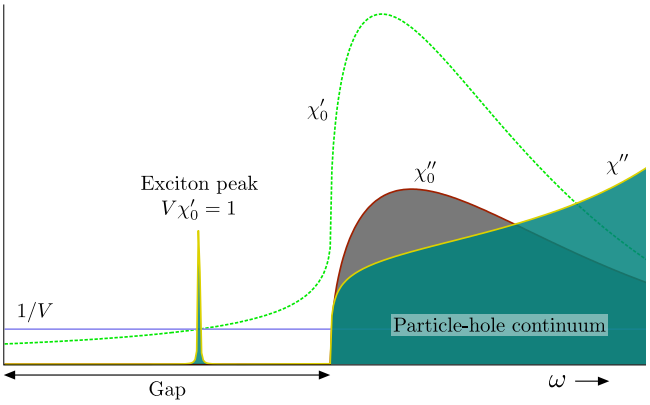

Figure 4.4: For small exciton coupling the spectrum of an exciton is obtained by the ladder diagram approximation from the spectrum of the single doped hole. The χ_0'' and χ_0' are respectively the imaginary and real part of the bare exciton susceptibility. The χ'' is the imaginary part of the full exciton susceptibility obtained in the ladder diagram approximation (4.15). Besides the continuous particle-hole spectrum above the gap, there can only be a single exciton peak determined by $V\chi_0' = 1$ in the weak coupling limit.

The bilayer $t - J$ model (4.14) describes generally the p/n-doped bilayer antiferromagnet. The behavior of a bound exciton, however, depends on the magnitude of the Coulomb force V in H_V, equation (4.13). If this Coulomb repulsion is relatively weak, the motion of holons and doublons will be rather independent of each other and the H_V can be treated as a perturbation on

$H_t + H_J$. The full **exciton-susceptibility** $\chi(\omega)$ can be obtained from the bare susceptibility $\chi_0(\omega)$ in the absence of the Coulomb force using the ladder diagram approximation,

$$\chi(\omega) = \frac{\chi_0(\omega)}{1 - V\chi_0(\omega)}. \tag{4.15}$$

Since the undoped state is a Mott insulator, there is a gap in the imaginary part of the bare susceptibility χ_0''. Above this gap there is an onset of the particle-hole continuum. In the ladder diagram approximation, there can only be a single delta function peak in the full susceptibility at $V\chi_0' = 1$ signaling the formation of an exciton. We conclude that in the weak coupling limit no special exciton features other than a single delta function peak can appear in the gap. Following our expectation that realistic materials are in fact in the strong coupling limit we will henceforth focus our attention to the strong coupling limit.

In the **strong coupling limit** ($V \gg t$), the hopping term H_t can be treated as a perturbation on the unperturbed H_V using the perturbation method developed by Kato,[16] in a manner similar to the derivation of the $t - J$ model from the Hubbard model in the previous section 4.1.1.[17] In the limit of strong V we consider the interlayer Coulomb interaction H_V, which has eigenvalues

[16] Kato, 1949

[17] Klein and Seitz, 1973; Takahashi, 1977; and Chao et al., 1977

$$E_{\widetilde{N}} = V(N - N_0 + \widetilde{N}) = E_0 + V\widetilde{N} \tag{4.16}$$

where N is the total number of sites, N_0 is the number of dopants per layer and $\widetilde{N}$ is the number of double occupied sites that do not lie above a vacant site. It is clear that the ground state of H_V is given by the state where all double occupied and vacant sites lie above each other, as depicted in figure 4.1. As mentioned before an **exciton** consists of a double occupied and a vacant site bound on top of each other. Consequently, the ground state of H_V is the state where all dopants are bound into excitons.

The essence of Kato's perturbation method is that we now forbid all states with higher H_V eigenvalues. This implies that we forbid states such as the one depicted in figure 4.5 where the double occupied site is not on top of the vacant site. In zeroth order, hopping of electrons is forbidden since that would break up an exciton state. Therefore the zeroth order Hamiltonian only contains Heisenberg terms $H_{\text{eft}}^{(0)} = H_J$.

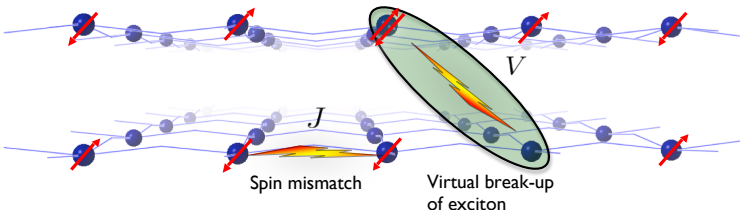

Figure 4.5: The motion of the composite exciton can be related to the motion of its constituents via Kato's perturbation method. In this method a virtual intermediate breakup of the exciton is in between the initial state (figure 4.1) and the final state (figure 4.3). The kinetic energy of the exciton is therefore the product of the kinetic energies of the holon and doublon divided by the energy of this virtual state, $t_{ex} = t_e t_h / V$.

In second order we consider intermediate processes that virtually break up excitons, as shown in figure 4.5. The corresponding effective Hamiltonian is given by

$$-\frac{1}{2V}\mathbf{P}_e H_t (1-\mathbf{P}_e) H_t \mathbf{P}_e \tag{4.17}$$

where $\mathbf{P}_e$ is the operator that projects out states with unbound dopants. Let us define the exciton operator in terms of electron creation operators

$$E_i^\dagger = c_{i1\uparrow}^\dagger c_{i1\downarrow}^\dagger (1-\rho_{i2}), \tag{4.18}$$

where $\rho_{i2} = \sum_\sigma c_{i2\sigma}^\dagger c_{i2\sigma}$ is the density operator in the p-type layer. The perturbation theory now yields an exciton hopping term, which can be formulated as

$$H_{t,ex} = -\frac{t_e t_h}{V} \sum_{<ij>\sigma\sigma'} E_j^\dagger \left[c_{i1\sigma'}^\dagger c_{i2\sigma}^\dagger c_{j2\sigma} c_{j1\sigma'} \right] E_i \tag{4.19}$$

Note that in this Hamiltonian, no break-up of the exciton is required. The virtual process as described before enables us to relate the single layer kinetic energies to the bilayer exciton kinetic energy,

$$t = \frac{t_e t_h}{V}. \tag{4.20}$$

Here t_e is the hopping energy for a single electron, t_h the hopping energy for a single hole and t is the hopping energy for a bound exciton. In addition to this hopping process there are also second order processes that equal a shift in chemical potential of the excitons.

Hence the strong coupling limit of H_V describes the motion of bound excitons in a Mott insulator double layer. The corresponding Hamiltonian is

$$H = H_{t,ex} + H_J \tag{4.21}$$

We will refer to this model as the **exciton $t-J$ model**.

The hopping term (4.19) represents an exciton E_i on site i swapping places with the spin background $c_{jp\sigma}c_{jn\sigma'}$ on site j. This Hamiltonian is in the electron Fock state representation with the background determined by the bilayer Heisenberg model (4.12). Unlike the fermionic holes in the single layer case, the exciton is composed of a fermionic doublon and holon in the same rung, and hence is a bosonic particle. We can therefore rewrite the Hamiltonian in terms of **bosonic operators**. The local Hilbert space on each interlayer rung is five dimensional with a basis in terms of five hard-core bosons: one interlayer exciton state $|E\rangle_i$ and four different spin states. In the **singlet-triplet basis**, which is valid for both the doped and undoped case, we cast the exciton $t-J$ model explicitly in a purely bosonic language. The four hard core spin bosons are one singlet state and three triplet states,

$$|0\ 0\rangle_i = \frac{1}{\sqrt{2}}(c^\dagger_{i1\uparrow}c^\dagger_{i2\downarrow} - c^\dagger_{i1\downarrow}c^\dagger_{i2\uparrow})|0\rangle \tag{4.22}$$

$$|1\ 0\rangle_i = \frac{1}{\sqrt{2}}(c^\dagger_{i1\uparrow}c^\dagger_{i2\downarrow} + c^\dagger_{i1\downarrow}c^\dagger_{i2\uparrow})|0\rangle \tag{4.23}$$

$$|1\ 1\rangle_i = c^\dagger_{i1\uparrow}c^\dagger_{i2\uparrow}|0\rangle \tag{4.24}$$

$$|1\ -1\rangle_i = c^\dagger_{i1\uparrow}c^\dagger_{i2\uparrow}|0\rangle. \tag{4.25}$$

The hopping term (4.19) can be re-expressed as:

$$H_{t,ex} = -t\sum_{<ij>}|E_j\rangle\left(|0\ 0\rangle_i\langle 0\ 0|_j + \sum_m |1\ m\rangle_i\langle 1\ m|_j\right)\langle E_i|. \tag{4.26}$$

We can introduce the total spin operator

$$\mathbf{S}_i = \mathbf{s}_{i1} + \mathbf{s}_{i2} \tag{4.27}$$

and the spin difference operator

$$\widetilde{\mathbf{S}} = \mathbf{s}_{i1} - \mathbf{s}_{i2}. \tag{4.28}$$

Explicitly in terms of singlet and triplet rung states for $S = \frac{1}{2}$, this reads[18]

[18] van Duin and Zaanen, 1997

$$S^z_i = |1\ 1\rangle\langle 1\ 1| - |1\ -1\rangle\langle 1\ -1| \tag{4.29}$$

$$S^+_i = \sqrt{2}\,(|1\ 1\rangle\langle 1\ 0| + |1\ 0\rangle\langle 1\ -1|) \tag{4.30}$$

$$\widetilde{S}^z_i = -|0\ 0\rangle\langle 1\ 0| - |1\ 0\rangle\langle 0\ 0| \tag{4.31}$$

$$\widetilde{S}^+_i = \sqrt{2}\,(|1\ 1\rangle\langle 0\ 0| - |0\ 0\rangle\langle 1\ -1|)\,. \tag{4.32}$$

In general, we see that the operator $\mathbf{S}_i$ conserves the total onsite spin, while $\widetilde{\mathbf{S}}$ always changes the total spin number s by a unit. The z-components of the spin operators do not change the magnetic number m, while the $\pm$-components of the spin operators change the magnetic number by a unit. The bilayer Heisenberg model is now written as

$$H_J = \frac{J}{2}\sum_{\langle ij\rangle}\left(\mathbf{S}_i\cdot\mathbf{S}_j + \widetilde{\mathbf{S}}_i\cdot\widetilde{\mathbf{S}}_j\right) + \frac{J_\perp}{4}\sum_i\left(\mathbf{S}_i^2 - \widetilde{\mathbf{S}}_i^2\right). \tag{4.33}$$

From now on we will study the **exciton t-J model in the singlet-triplet basis**, which is given by the hopping term (4.26) and the Heisenberg terms (4.33).

4.1.4 *Sign problem*

Notice that the Hilbert space no longer contains fermionic degrees of freedom. The question is whether the disappearance of the fermionic structure also leads to the disappearance of the fermionic **sign structure**, which causes so much difficulties in the single layer $t-J$ model.[19]

[19] Wu et al., 2008

The sign structure can be investigated by considering the off-diagonal matrix elements of the Hamiltonian. At half-filling the fermionic signs in the standard $t-J$ model on a bipartite lattice can be removed by a Marshall sign transformation.[20] Upon doping, signs reappear whenever a hole is exchanged with (for example) a down spin. Which matrix elements of the Hamiltonian become positive (and thus create a minus sign in the path integral loop expansion) depends on the specific basis and on the specific Marshall sign transformation.

[20] Marshall, 1955

For the double layer exciton model, define a spin basis state with a built-in Marshall sign transformation of the form[21]

[21] Compare to Weng, 2007.

$$|\phi\rangle = (-1)^{N_{An}^{\downarrow}+N_{Bp}^{\downarrow}}\left|\begin{array}{ccccc}\cdots & \downarrow & \uparrow\downarrow & \uparrow & \cdots\\ & \downarrow & 0 & \downarrow & \end{array}\right\rangle \tag{4.34}$$

where $N_{An}^{\downarrow}$ is the number of down spins on the A sublattice in the n-layer and similarly we define $N_{Bp}^{\downarrow}$. With these basis states the Heisenberg terms are sign-free and the only positive matrix elements come from the exchange of an exciton with a $m=\pm1$ triplet.

We conclude that, even though the model is purely bosonic, the exciton $t - J$ model is not sign-free and it is not possible to remove this sign structure using a Marshall or similar transformation.[22] However, as will be further elaborated upon in section 4.2.2, for both the antiferromagnetic and singlet ground states these signs do cancel out. Therefore for such ordered bilayers the problem of exciton motion turns out to be effectively bosonic.

[22] We are not claiming that the sign structure cannot be removed. Of course, if we would know the exact eigenstates of the Hamiltonian there would be no sign problem. However, finding a basis where the sign structure vanishes is in general a NP-hard problem (Troyer and Wiese, 2005).

4.2 *Frustration of a single exciton in an antiferromagnet*

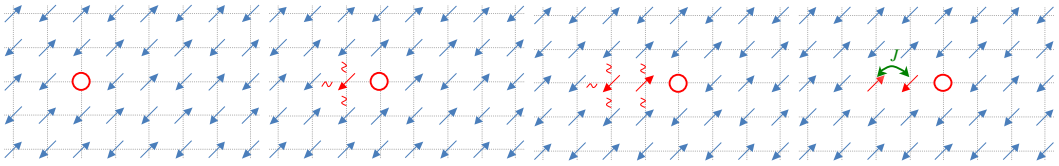

Figure 4.6: A moving hole in an antiferromagnet creates a string of upturned spins. With increasing distance the energy associated with the frustrated bonds increases, which leads to confinement of the hole to its initial position. Upon inclusion of quantum JS^+S^- corrections, the hole can still move, albeit with renormalized bandwidth.

The discovery of high T_c superconductivity triggered a concerted theoretical effort aimed at understanding the physics of doped Mott insulators.[23] Although much is still in the dark, the problem of **an isolated carrier in the insulator** is regarded as well understood.[24] It turned out to be a remarkable affair, rooted in the quantum-physical conflict between the antiferromagnetism of the spin system and the delocalizing carrier. This conflict is at its extreme dealing with a classical Ising spin system, where a famous cartoon arises for the idea of confinement (see figure 4.6): the hopping causes a 'magnetic string' of overturned spins between the delocalizing charge and the spin left at the origin with an exchange energy increasing linearly in their separation. It was realized that the quantummechanical nature of the $S = 1/2$ Heisenberg spin system changes this picture drastically. The quantum spin-corrections repair efficiently this 'confinement damage' in the spin background and one finds a 'spin-liquid polaron' as quasiparticle that propagates coherently through the lattice on a scale set by the exchange constant. This physics can be reliably addressed by parametrizing the spin system in terms of its linear spin waves (LSW), while the strong coupling between the spin waves and the propagating hole is well described in terms of the self consistent Born approximation (SCBA). This turned out to be accurate to a degree that the photoemission results in insulating

This section is based on Rademaker et al., 2012a and Rademaker et al., 2012b.

[23] Imada et al., 1998; and Lee et al., 2006

[24] Bulaevskii et al., 1968; Brinkman and Rice, 1970; Schmitt-Rink et al., 1988; Kane et al., 1989; Martinez and Horsch, 1991; and Dagotto, 1994

cuprates were quantitatively explained in this framework.[25]

A related problem is the delocalization of an exciton (bound electron-hole pair, or more exactly the bound state of a double occupied and vacant site) through the antiferromagnetic background. It is easy to see that the propagation of an **exciton in a single layer** is barely affected by the antiferromagnetism since the combined motion of the electron and the hole neutralize the 'damage' in the spin system.[26] A problem of interest for this thesis is the exciton formed in a bilayer, where the electron and the hole reside in the different layers. Here we report the discovery that such **bilayer excitons** couple extremely strongly through their quantum motion to the spin system.

[25] Damascelli et al., 2003

[26] Zhang and Ng, 1998

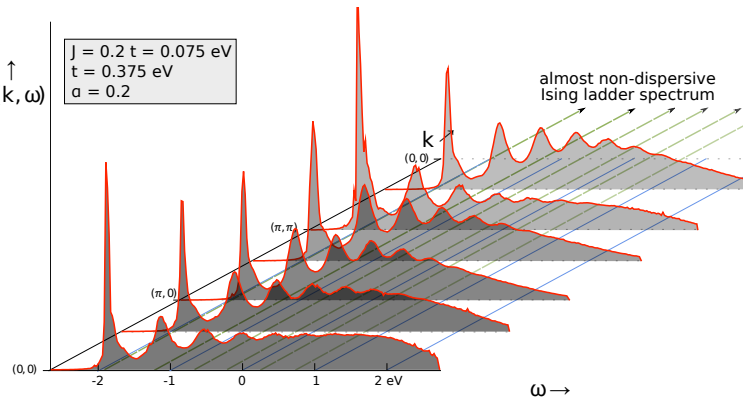

Figure 4.7: Exciton spectral function for $J = 0.2t$ and $\alpha = 0.2$. On top of the incoherent bump a strong ladder spectrum has developed, signaling Ising confinement. The exact Ising ladder spectrum is shown in green dotted lines. The Ising peaks are very weakly dispersive, with bandwidth of order J.

In fact, when the interlayer exchange coupling is small and the exciton hopping rate is large, one enters a regime that is similar to the **confinement** associated with the Ising spins, although the spin system is in the quantized Heisenberg regime. This is illustrated by the exciton spectral function shown in figure 4.7 as computed with the LSW-SCBA method, showing the non-dispersive 'ladder spectrum' which is a fingerprint of confinement. Figure 4.3 depicts a cartoon of the confinement mechanism: every time the exciton hops it creates two spin flips in the different layers that can only be repaired by quantum spin superexchange driven by the interlayer exchange coupling. The rapid intralayer quantum spin flips are now ineffective, because the restoration of the antiferromagnetism requires quantum spin flips that occur simultaneously in the two layers with a probability that is strongly suppressed.

This confinement effect can be studied directly in experiment by measuring the exciton spectrum in **c-axis optical absorption of the $YBa_2Cu_3O_6$ (YBCO)** insulating bilayer system. Using realistic parameters we anticipate that this will look like figure 4.8: the main difference with figure 4.7 is that the exciton hopping rate is now of order of the exchange energy and in this adiabatic regime the spectral weight in the ladder spectrum states is reduced.

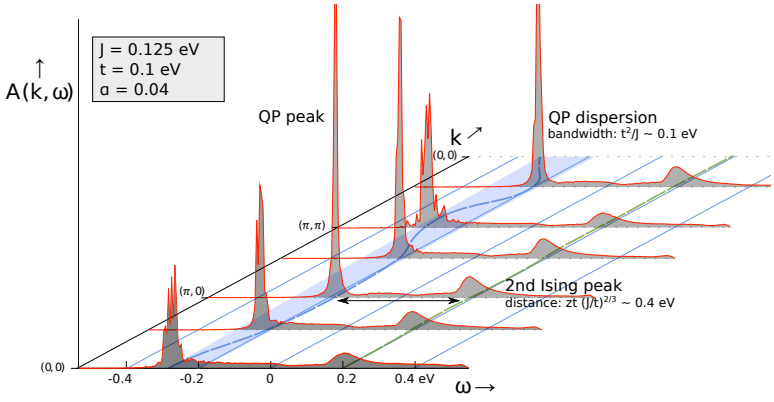

Figure 4.8: Expected exciton spectral function for the c-axis charge-transfer exciton in YBCO bilayers. We used model parameters $J = 0.125$ eV, $t = 0.1$ eV and $\alpha = 0.04$. The exciton quasiparticle peak has a dispersion with bandwidth t^2/J, and the quasiparticle peak is the most pronounced at the line between $(\pi, 0)$ and $(0, \pi)$. Following at a distance of $zt(J/t)^{2/3}$, a secondary peak develops as a sign of Ising confinement.

4.2.1 *Undoped case: the bilayer Heisenberg model*

As described in section 4.1, we need to derive a spin wave theory for the bilayer Heisenberg model before considering the dynamics of the exciton. Similar to the traditional Holstein-Primakoff spin-wave theory, we need a classical reference state, i.e. the mean field ground state of the bilayer Heisenberg model, and subsequently develop the linear corrections of the spin wave theory from the mean field ground state. The method we present here is similar to the one presented in Sommer et al., 2001.

The singlet-triplet basis (4.33) of the bilayer Heisenberg model is convenient for **mean field theory**. Mean field theory tells us that for large ratio $J_\perp/J$ the ground state is the singlet configuration $|0\ 0\rangle$. For small $J_\perp/J$, we expect antiferromagnetic ordering, which amounts to a staggered condensation of $\widetilde{S}^z$. By setting $\langle \widetilde{S}^z \rangle = (-1)^i \widetilde{m}$ we obtain a mean field Hamiltonian

$$H_J^{MF} = \sum_i \left[\frac{1}{4} J z \widetilde{m}^2 + \frac{J_\perp}{4} \left(S_i^2 - \widetilde{S}_i^2 \right) - \frac{1}{2} J z \widetilde{m} (-1)^i \widetilde{S}_i^z \right] \qquad (4.35)$$

which has a order-disorder transition point at

$$\alpha_c \equiv \left(\frac{J_\perp}{Jz}\right)_c = \frac{4}{3}S(S+1) \tag{4.36}$$

where S is the magnitude of spin of the spin operator on each site.[27]

[27] A proof of this result can be found in Rademaker et al., 2012b.

[28] Anderson, 1952; Kubo, 1952; and Dyson, 1956

The basic idea of a **spin wave theory**[28] is to start from this semiclassical (mean field) ground state and describe the local excitations with respect to this ground state. One can immediately infer why the Holstein-Primakoff or Schwinger approach to spin wave theories fails for the bilayer Heisenberg model. First, the mean field ground state is no longer a Néel state for finite α. Secondly, while Holstein-Primakoff describes one, and Schwinger describes two onsite spin excitations, the bilayer Heisenberg has in fact three types of excitations. This has been pointed out by Chubukov and Morr, 1995, who called the 'third' excitation the longitudinal mode.

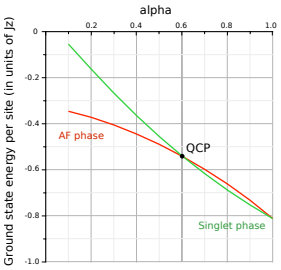

Figure 4.9: Ground state energies of the bilayer Heisenberg model, with the spin wave corrections included. At $\alpha \approx 0.605$ there is a phase transition from the antiferromagnetic phase (in red) to the singlet phase (in green).

With the mean field ground state as described by (4.35) we can 'reach' all states in the local Hilbert space with three types of excitations: a longitudinal $e^\dagger$ which keeps the magnetic quantum number m constant, and two transversal $b^\dagger_\pm$ who change m by ± 1. In the limit of large S these excitations tend to become purely bosonic. We will take the mean field ground state of (4.35) and these three excitations as the starting point for the linear spin wave theory.

We must mention the obvious flaw in the above reasoning. Where we criticized earlier spin wave theories because they predicted the wrong critical value of $J_\perp/Jz$, we now apparently adopt such a 'wrong' theory since (4.36) predicts $\alpha_c = 1$ for $S = \frac{1}{2}$! Nevertheless, the presence of spin waves changes the ground state energy which makes the disordered state more favorable even below the mean field critical $\left(\frac{J_\perp}{Jz}\right)_c$ calculated in the above, see figure 4.9. Hence, when the ground state energy shifts are taken into account in linear order, one finds an accurate critical value for α consistent with numerical calculations.

Let us now construct explicitly the spin wave theory described in the above for $S = \frac{1}{2}$. First, one needs to find the ground state according to equation (4.35). In the $S = \frac{1}{2}$ case, this amounts to a competition between the singlet state $|s = 0, m = 0\rangle$ and the triplet $|s = 1, m = 0\rangle$. The **mean field ground state on each rung**

is given by a linear superposition of those two,

$$|G\rangle_i = \eta_i \cos\chi |0\ 0\rangle_i - \sin\chi |1\ 0\rangle_i, \tag{4.37}$$

which interpolates between the Néel state ($\chi = \pi/4$) and the singlet state ($\chi = 0$). The onset of antiferromagnetic order can thus be viewed as the condensation of the triplet state in a singlet background.[29] With $\eta_i = (-1)^i$ alternating we have introduced a sign change between the two sublattices A and B. The angle χ will be determined later by self-consistency conditions.

[29] van Duin and Zaanen, 1997; and Sommer et al., 2001

The three operators that describe excitations with respect to the ground state are

$$e_i^\dagger = (\eta_i \sin\chi |0\ 0\rangle_i + \cos\chi |1\ 0\rangle_i)\, \langle G|_i, \tag{4.38}$$

$$b_{i+}^\dagger = |1\ 1\rangle_i \langle G|_i, \tag{4.39}$$

$$b_{i-}^\dagger = |1\ -1\rangle_i \langle G|_i. \tag{4.40}$$

The e-operators will later turn out to represent the longitudinal spin waves, whereas the b-operators represent the two possible transversal spin waves.

The bilayer Heisenberg model can be rewritten in terms of these operators. For completeness we include the parameter λ that enables a comparison with the Ising limit ($\lambda = 0$) with the Heisenberg limit ($\lambda = 1$),

$$\mathbf{S}_1 \cdot \mathbf{S}_2 = S_1^z S_2^z + \frac{1}{2}\lambda (S_1^+ S_2^- + S_1^- S_2^+). \tag{4.41}$$

Given this, we can explicitly write down the spin operators in terms of the new e and b operators,

$$S_{i\sigma}^z = b_{+i\sigma}^\dagger b_{+i\sigma} - b_{-i\sigma}^\dagger b_{-i\sigma} \tag{4.42}$$

$$S_{i\sigma}^+ = \sqrt{2}\left(-\sin\chi (b_{+i\sigma}^\dagger + b_{-i\sigma}) + \cos\chi (b_{+i\sigma}^\dagger e_{i\sigma} + e_{i\sigma}^\dagger b_{-i\sigma})\right) \tag{4.43}$$

$$\widetilde{S}_{i\sigma}^z = (-1)^{\sigma_i}\left(\sin 2\chi (1 - \sum_{\pm} b_{\pm i\sigma}^\dagger b_{\pm i\sigma} - 2 e_{i\sigma}^\dagger e_{i\sigma}) - \cos 2\chi (e_{i\sigma}^\dagger + e_{i\sigma})\right) \tag{4.44}$$

$$\widetilde{S}_{i\sigma}^+ = \sqrt{2}(-1)^{\sigma_i}\left(\cos\chi (b_{+i\sigma}^\dagger - b_{-i\sigma}) + \sin\chi (b_{+i\sigma}^\dagger e_{i\sigma} - e_{i\sigma}^\dagger b_{-i\sigma})\right). \tag{4.45}$$

From the requirement that the Hamiltonian does not contain terms linear in spin wave operators we obtain the self-consistent mean field condition for the ground state angle χ,

$$(\cos 2\chi - \alpha\lambda) \sin 2\chi = 0 \tag{4.46}$$

which has two possible solutions: either $\chi = 0$, which corresponds to a singlet ground state configuration (the **disordered phase**), or $\cos 2\chi = \alpha\lambda$ corresponding with an **antiferromagnetic ordered phase**. These are indeed the two phases represented in figure 4.2. Which of the two solutions ought to be chosen, depends on the ground state energy competition. In figure 4.9 we compare the ground state energy of both phases, from which we can deduce that the critical point lies at $\alpha_c \approx 0.6$, consistent with the numerical literature.[30]

[30] Sandvik et al., 1995; and Sandvik and Scalapino, 1994

The dispersion of the spin wave excitations can be found when we consider only the quadratic terms in the Hamiltonian. This is called the **'linear' spin wave approximation**, and it amounts to neglecting the cubic and quartic interaction terms. First take a Fourier transform of the spin wave operators

$$e^\dagger_{i\sigma} = \sqrt{\frac{2}{N}} \sum_k e^\dagger_{k\sigma} e^{ik\cdot r_i} \tag{4.47}$$

where the sum over k runs over the $2/N$ momentum points in the domain $[-\pi, \pi] \times [-\pi, \pi]$ and $\sigma = A, B$ represents the sublattice index. A similar definition is used for the b-operators.

Upon Fourier transformation, we can decouple the spin waves from the two sublattices A and B by introducing

$$e^\dagger_{k,p} = \frac{1}{\sqrt{2}}(e^\dagger_{kA} + p e^\dagger_{kB}) \tag{4.48}$$

where $p = \pm$ stand for the phase of the spin mode. Modes with $p = -1$ are out-of-phase and have the same dispersion as the in-phase $p = 1$ modes but shifted over the antiferromagnetic wavevector $Q = (\pi, \pi)$. Similar considerations apply to the b operators.

Next we perform the **Bogolyubov transformation** on the magnetic excitations,

$$e^\dagger_{k,p} = \cosh \varphi_{k,p} \zeta^\dagger_{k,p} + \sinh \varphi_{k,p} \zeta_{-k,p} \tag{4.49}$$

$$b^\dagger_{k,p,+} = \cosh \theta_{k,p} \alpha^\dagger_{k,p} + \sinh \theta_{k,p} \beta_{-k,p} \tag{4.50}$$

$$b^\dagger_{k,p,-} = \cosh \theta_{k,p} \beta^\dagger_{k,p} + \sinh \theta_{k,p} \alpha_{-k,p} \tag{4.51}$$

The corresponding transformation angles are set by the requirement that the Hamiltonian becomes diagonal in the new operators ζ (the longitudinal spin wave) and α, β (the transversal spin waves).

In doing so, we introduced the **'ideal' spin wave approximation** in which we assume that the spin wave operators obey bosonic commutation relations.[31] This assumption is exact in the large S limit. For $S = \frac{1}{2}$ this approximation turns out to work extremely well,[32] since the corrections to the bosonic commutation relations are expressed as higher order spin-wave interactions. The Bogolyubov angles are given by

[31] Dyson, 1956

[32] Manousakis, 1991

$$\tanh 2\varphi_{k,p} = \frac{-p\frac{1}{2}\cos^2 2\chi\gamma_k}{\sin^2 2\chi + \lambda\alpha\cos 2\chi - p\frac{1}{2}\cos^2 2\chi\gamma_k}, \quad (4.52)$$

$$\tanh 2\theta_{k,p} = \frac{p\lambda\gamma_k}{\sin^2 2\chi + (1+\lambda)\alpha\cos^2\chi - p\lambda\cos 2\chi\gamma_k} \quad (4.53)$$

The factor γ_k encodes for the lattice structure, and it equals for a square lattice

$$\gamma_k = \frac{1}{z}\sum_{\delta} e^{ik\cdot\delta} = \frac{1}{2}\left(\cos k_x + \cos k_y\right) \quad (4.54)$$

where the sum runs over all nearest neighbor lattice sites δ. The Bogolyubov angles still depend on χ, which characterizes the ground state. In the antiferromagnetic phase $\cos 2\chi = \lambda\alpha$ and for the Heisenberg limit $\lambda = 1$ these angles reduce to

$$\tanh 2\varphi_{k,p} = \frac{-p\alpha^2\gamma_k}{2 - p\alpha^2\gamma_k}, \quad (4.55)$$

$$\tanh 2\theta_{k,p} = \frac{p\gamma_k}{1 + \alpha - p\alpha\gamma_k}. \quad (4.56)$$

We can distinguish between the **longitudinal** and **transversal spin excitations**, with their dispersions given by

$$\epsilon^L_{k,p} = Jz\sqrt{1 - p\alpha^2\gamma_k} \quad (4.57)$$

$$\epsilon^T_{k,p} = \frac{1}{2}Jz\sqrt{(1+\alpha(1-p\gamma_k))^2 - \gamma_k^2} \quad (4.58)$$

The longitudinal spin wave is gapped and becomes in the limit where the layers are decoupled ($\alpha = 0$) completely non-dispersive, while the transversal spin wave is always linear for small momentum k. This type of spectrum is similar to a phonon spectrum, which contains a linear k-dependent acoustic mode and a gapped flat optical mode. This correspondence between spin waves and phonons enables us to use techniques from electron-phonon interaction studies for the exciton-spin wave interactions.

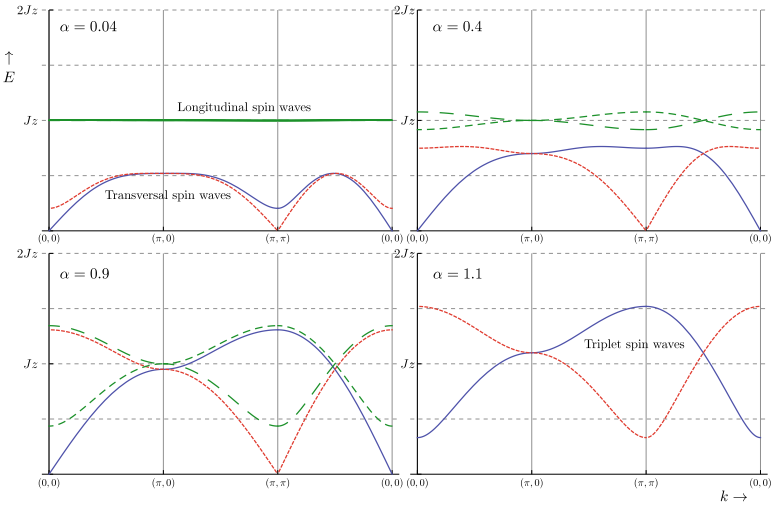

Figure 4.10: Dispersion of the bilayer Heisenberg spin waves for different values of α. The top row has $\alpha = 0.04$ and $\alpha = 0.4$, the bottom row $\alpha = 0.9$ and $\alpha = 1.1$. In the antiferromagnetic phase (first three pictures) there is a clear distinction between the longitudinal spin waves (long dashed lines in green) and the transversal spin waves (solid line in blue; and the short dashed in red). The first is gapped, whilst the latter is zero at either $k = (0,0)$ or (π,π) with a linear energy-momentum dependence. In the singlet phase, all spin waves are gapped triplet excitations (depicted as solid blue line and dashed red line).

On the other hand, in the singlet phase ($\alpha > 1$) one has trivially three identical **triplet spin excitations**. The Bogolyubov angles are given by

$$\tanh 2\varphi_{k,p} = -\tanh 2\theta_{k,p} = \frac{-p\gamma_k}{2\alpha - p\gamma_k} \tag{4.59}$$

and the dispersion of the triplet spin waves is

$$\epsilon_{k,p} = Jz\sqrt{\alpha(\alpha - p\gamma_k)}. \tag{4.60}$$

These dispersions correspond to earlier numerical and series expansions results.[33] In fact, these results are exactly equal to the dispersions obtained in the non-linear sigma model.[34]

The above derivation adds to earlier studies of the bilayer Heisenberg model in that we now found explicit expressions of how the spin waves are related to local spin flips, equations (4.49)-(4.53). This microscopic understanding of the magnetic excitations of the system enables us in the next section to derive how magnetic interactions influence the dynamics of excitons.

[33] Kotov et al., 1998; Weihong, 1997; Gelfand, 1996; and Chubukov and Morr, 1995

[34] van Duin and Zaanen, 1997

4.2.2 *A single exciton in a correlated bilayer*

We are now in the position to derive the **dynamics of a single exciton** in the undoped bilayer. Note that in the thermodynamic limit a single exciton will not change the ground state. Following

the exciton hopping Hamiltonian (4.26) we can express the dynamics of the exciton upon interaction with the spin wave modes. A single exciton can be physically realized by either exciting a interlayer charge-transfer exciton in the undoped bilayer, or by infinitesimal small chemical doping of layered structures.

Similar to the single layer case,[35] we consider the mean field state $|G\rangle$ as the vacuum state and from there we write the effective hopping Hamiltonian for a single exciton as

[35] Schmitt-Rink et al., 1988

$$H_{t,ex} = t \sum_{\langle ij \rangle} E_j^\dagger E_i \left[\cos 2\chi (1 - e_i^\dagger e_j) + \sin 2\chi (e_i^\dagger + e_j) - \sum_\sigma b_{i\sigma}^\dagger b_{j\sigma} \right] + h.c.. \tag{4.61}$$

The dynamics of a single exciton are contained in the **dressed Greens function**, formally written as

$$G^p(k,\omega) = \langle \psi_0 | E_{k,p} \frac{1}{\omega - H + i\epsilon} E_{k,p}^\dagger | \psi_0 \rangle \tag{4.62}$$

where $E_{k,p}^\dagger$ is the Fourier transformed exciton creation operator, and p indicates the same phase index as used for the spin waves in equation (4.48). The $|\psi_0\rangle$ denotes the ground state that arises from the spin wave approximation,[36] hence $|\psi_0\rangle$ is defined by the conditions

[36] Manousakis, 1991

$$\zeta_{k,p} |\psi_0\rangle = \alpha_{k,p} |\psi_0\rangle = \beta_{k,p} |\psi_0\rangle = 0 \tag{4.63}$$

for all k, p. Note that $|\psi_0\rangle$ is not equal to the mean field ground state $|G\rangle$ defined in equation (4.37).

The Greens function cannot be solved exactly and one needs to develop a diagrammatic expansion in the parameter t. For this purpose, we have derived the corresponding Feynman rules of the exciton $t - J$ model, see appendix D of Rademaker et al., 2012b.

Using **Dyson's equation** one can rephrase the diagrammatic expansion in terms of the self-energy $\Sigma^p(k,\omega)$ such that

$$G^p(k,\omega) = \frac{1}{\omega - \epsilon_0^p(k) - \Sigma^p(k,\omega) + i\epsilon} \tag{4.64}$$

where $\epsilon_0^p(k)$ is the dispersion in the absence of spin excitations for the exciton with phase p. The self-energy can be computed by summing all one-particle irreducible Feynman diagrams. The degree to which exciton motion contains a free part grows with α, and indeed the free dispersion is

$$\epsilon_0^p(k) = p\, zt \cos 2\chi\, \gamma_k \tag{4.65}$$

where $\cos 2\chi$ equals $\alpha\lambda$ in the antiferromagnetic phase and equals 1 in the singlet phase.

As we noted before, the spin wave spectrum resembles a phonon spectrum. Hence we can compute the exciton self-energy using the **Self-Consistent Born Approximation (SCBA)**,[37] an approximation scheme developed for electron-phonon interactions but subsequently successfully applied to the single layer $t-J$ model.

[37] Schmitt-Rink et al., 1988; and Kane et al., 1989

The SCBA is based on two assumptions: 1) that one can neglect vertex corrections and 2) one uses only the bare spin wave propagators. The first assumption is motivated by an extension of **Migdal's theorem**. For electron-phonon interaction, higher order vertex corrections are of order $\frac{m}{M}$ where m is the electron mass and M is the ion mass. This justifies that for electron-phonon interactions the SCBA is right.[38] Comparisons between the SCBA and exact diagonalization methods for the single layer $t-J$ model have shown that it is justified to neglect the vertex correction there as well.[39] The second assumption is motivated by the linear spin wave approximation. Consequently, all remaining diagrams are of the 'rainbow' type which can be summed over using a self-consistent equation. The assumption that the vertex corrections are irrelevant allows us to completely resum Feynman diagrams up to all orders in t. The SCBA is therefore not a perturbation series expansion and consequently t does not necessarily has to be a small parameter.

[38] Fetter and Walecka, 2003

[39] Martinez and Horsch, 1991

For the exciton $t-J$ model, the SCBA amounts to computing the self-energy for the in-phase exciton, as shown diagrammatically in figure 4.11. The usual Feynman rules dictate that we need to integrate over all intermediate frequencies of the virtual spin waves. However, under the linear spin wave approximation the spin wave propagator is $i/(\omega' - \epsilon(k) + i\epsilon)$ which amounts to a Dirac delta function in the frequency domain integration.[40] For example, the first diagram of figure 4.11 is reduced as follows,

[40] Schmitt-Rink et al., 1988

$$\frac{1}{N}\sum_{q,p}\int_{-\infty}^{\infty}\frac{d\omega'}{\pi}M_{k,q}^2 G^p(k-q,\omega-\omega')\left[\frac{i}{\omega'-\epsilon_{k,p}^L+i\epsilon}\right] = \frac{1}{N}\sum_{q,p}M_{k,q}^2 G^p(k-q,\omega-\epsilon_{q,p}^L), \quad (4.66)$$

where $M_{k,q}$ is the vertex contribution and $G^p(k,\omega)$ is the exciton

propagator. Emission (or absorption) of a spin wave by an exciton can thus be incorporated by changing the momentum and energy of the exciton propagator. Analytically we write for the in-phase **exciton self-energy**,

$$\begin{aligned}\Sigma^{+}(k,\omega) = \frac{z^2t^2}{N}\sin^2 2\chi \sum_{q,p}\left(\gamma_{k-q}\cosh\varphi_{q,p} + p\gamma_k \sinh\varphi_{q,p}\right)^2 G^{p}(k-q,\omega-\epsilon^{L}_{q,p}) \\ + \frac{z^2t^2}{N^2}\cos^2 2\chi \sum_{q,q'}\sum_{\pm,p}\left(\gamma_{k+q'}\cosh\varphi_{q,p}\sinh\varphi_{q',\pm p} \pm \gamma_{k+q}\cosh\varphi_{q',\pm p}\sinh\varphi_{q,p}\right)^2 \\ \times G^{\pm}\left(k-q-q',\omega-\epsilon^{L}_{q,p}-\epsilon^{L}_{q',\pm p}\right) \\ + \frac{z^2t^2}{N^2}\sum_{q,q'}\sum_{\pm,p}\left(\gamma_{k-q}\cosh\theta_{q,p}\sinh\theta_{q',\pm p} \pm \gamma_{k-q'}\cosh\theta_{q',\pm p}\sinh\theta_{q,p}\right)^2 \\ \times G^{\pm}\left(k-q-q',\omega-\epsilon^{T}_{q,p}-\epsilon^{T}_{q',\pm p}\right) \qquad (4.67)\end{aligned}$$

which depends on the exciton propagator and the Bogolyubov angles derived in the previous section. A similar formula to (4.67) applies to Σ^{-}. However, it is easily verified that

$$\Sigma^{-}(k,\omega) = \Sigma^{+}(k+(\pi,\pi),\omega) \qquad (4.68)$$

since $\gamma_{k+(\pi,\pi)} = -\gamma_k$. In general the SCBA (4.67) cannot be solved analytically, and hence we have obtained the exciton spectral function

$$A(k,\omega) = -\frac{1}{\pi}\mathrm{Im}\left[G(k,\omega)\right] \qquad (4.69)$$

using an iterative procedure with Monte Carlo integration over the spin wave momenta discretized on a 32×32 momentum grid. We start with $\Sigma = 0$ and after approximately 20 iterations the spectral function converged. The results for typical values of α, J and t are shown in figures 4.12 to 4.15.

We start from the situation with $\alpha > 1$ where the magnetic background is a **disordered phase** with all spin singlet configuration in

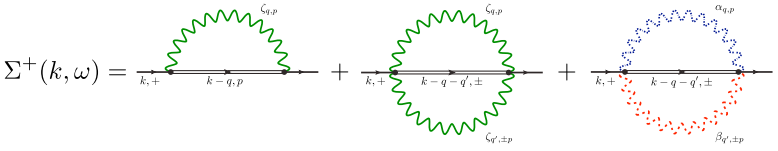

Figure 4.11: Feynman diagram representation of the Self-Consistent Born Approximation (SCBA) of equation (4.67). The self-energy of the exciton depends self-consistently on 'rainbow' diagrams where it emits and absorbs either one or two spin waves. The left two diagrams contain interaction with the longitudinal spin wave (solid green wavy propagators with ζ labels). The diagram to the right contains the interaction with the transversal spin waves; where the dotted (blue, upper, wavy) propagator denotes the α spin wave and the dashed (red, lower, wavy) propagator denotes the β spin wave. The definitions of ζ, α and β are given in equations (4.49)-(4.51). Note that vertex corrections are neglected in the SCBA.

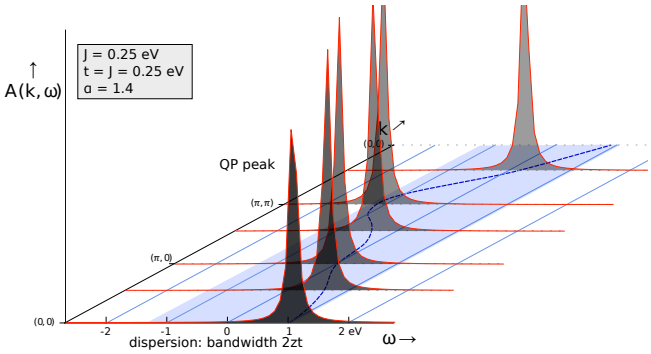

Figure 4.12: Exciton spectral function for parameters $J = t$ and $\alpha = 1.4$. The only relevant feature is the strong quasiparticle peak with dispersion equal to $8t$, where t is the hopping energy of the exciton. The horizontal axis describes energy, the vertical axis is the spectral function in arbitrary units.

the same rung. In this case, the free dispersion of the exciton with bandwidth proportional to t survives because all the magnetic triplet excitations are gapped, with a gap energy of $Jz\sqrt{\alpha(\alpha-1)}$. For $t < J$, the exciton-magnetic interactions will barely change the free dispersion while for $t > J$ such exciton-magnetic interactions can still occur, leading to a small 'spin polaron' effect where the exciton quasiparticle (QP) peak is diminished and spectral weight is transferred to a polaronic bump at a higher energy than the quasiparticle peak. For most values of t/J this effect is, however, negligible already for α just above the critical point. The exciton spectral function for $t = J$ and $\alpha = 1.4$ can be seen in figure 4.12.

As α decreases towards the **quantum critical point** at $\alpha = 1$, the gap of the triplet excitations also decreases. The effect of the exciton-magnetic interactions become more significant, which leads to an increasing transfer of spectral weight from the free coherent peak to the incoherent parts. When α hits the quantum critical point the gap to all spin excitations vanishes. There the motion of the exciton is strongly scattered by the spin excitations, completely destroying the coherent peak and leading to an incoherent critical hump in the spectrum as shown in figure 4.13. When α further decreases to values $\alpha < 1$, the magnetic background becomes antiferromagnetically ordered with two gapless transverse modes and one gapped longitudinal mode. In this case, the motion of the exciton is still strongly scattered with the spin excitations leaving a footprints in the exciton spectrum.

A most **striking phenomenon happens at** $\alpha = 0$, when the two layers are effectively decoupled and we would expect a similar behavior for an interlayer exciton as for a hole or electron in a single

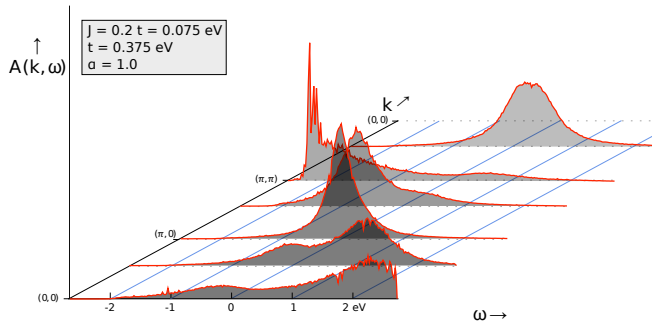

Figure 4.13: Exciton spectral function at the quantum critical point, for $J = 0.2t$ and $\alpha = 1$. No distinct quasiparticle peak is observable, and at all momenta a broad critical bump appears in the spectrum.

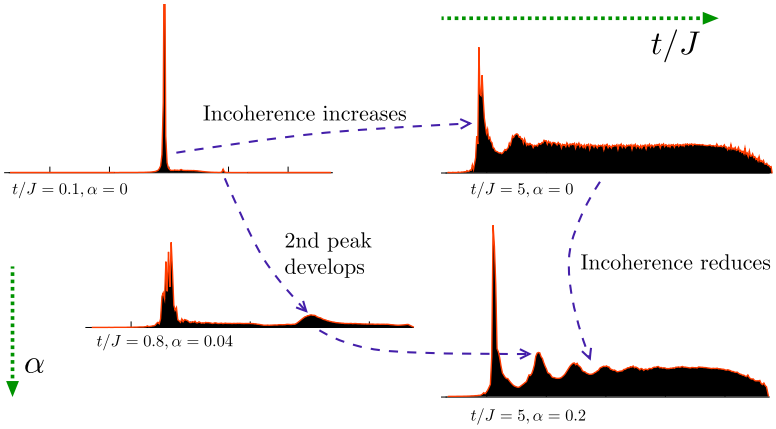

Figure 4.14: A qualitative overview of zero momentum exciton spectral functions $A(k = 0, \omega)$ for various parameters of t/J and small interlayer coupling α. For α identically zero, the ratio t/J determines the amount of excited spin waves. In the adiabatic limit $t \ll J$ no spin waves can be excited by and the exciton is localized with a clear quasiparticle peak. Upon increase of t/J more and more spectral weight is transferred to higher order spin wave peaks, which in the anti-adiabatic limit $t \gg J$ leads to the formation of a broad incoherent spectrum. The inclusion of a small nonzero interlayer coupling α reduces the incoherence of this spectrum, see equation (4.71). As a result the Ising-like ladder spectrum becomes more pronounced. Here we only show the zero momentum spectra, in figures 4.7, 4.8, 4.12, and 4.13 the momentum dependence of these spectra is shown.

layer. Indeed conform with the single hole in the $t - J$ model[41] we find that a moving exciton causes spin frustration with an energy proportional to J. In the limit where $J \gg t$ the kinetic energy of the exciton becomes too small for it to propagate coherently through the magnetic background. Therefore, we expect a localization of the exciton which is reflected in the spectral data by an almost non-dispersive quasiparticle peak. This peak has a bandwidth proportional to t^2/J and carries most of the spectral weight, $1 - \mathcal{O}(t^2/J^2)$. The remaining spectral weight is carried by a second peak, at an energy Jz above the main peak.

More complex behavior at $\alpha = 0$ arises in the **anti-adiabatic limit** $t \gg J$, where the kinetic energy of the exciton is large compared to the energy required to excite (and absorb) spin waves. Consequently, many spin waves are excited as the exciton moves and the exciton becomes 'overdressed' with multiple spin waves.

[41] Schmitt-Rink et al., 1988; and Kane et al., 1989

At nonzero J, however, a very small quasiparticle peak remains with a bandwidth of order J. Nonetheless the majority of spectral weight is carried in the incoherent many-spin wave part.

However, **realistic physical systems** are expected to have a small nonzero value of α and an intermediate value of t/J. What happens here? A simple extrapolation of the two aforementioned cases yields that the bandwidth of the quasiparticle peak will reach its maximum value at $J \approx t$. Similar extrapolations suggest that about half of the spectral weight will be carried by the QP peak. However, inclusion of a finite value of α is not so trivial on an analytical level. Numerical results are therefore needed, and an overview of spectral functions for different ratios of t/J and small values of α is given in figure 4.14.

4.2.3 *The mechanism of Ising-like confinement*

Upon the inclusion of a small nonzero interlayer coupling α a ladder spectrum seems to appear, reminiscent of the spectrum of a single hole in a Ising antiferromagnet. Physically, this can be understood as follows. In the $\alpha = 0$ limit, the magnetic interactions are dominated by the transverse excitations which are just single layer spin waves. For any finite $\alpha > 0$ the (interlayer) longitudinal spin waves become increasingly relevant. To understand their effect on the exciton spectral function, consider the SCBA equation (4.67), neglect the diagrams involving transversal spin waves and expand the self-energy up to first order in α. Only the single spin wave diagram contributes and it equals

$$\Sigma^{+}(k,\omega) = \frac{z^2 t^2}{N} \sum_{q,\pm} \gamma^2_{k-q} G^{\pm}(k-q, \omega - Jz) \tag{4.70}$$

from which we deduce, observing that $\Sigma^{-} = \Sigma^{+}$ and shifting the momentum summation, that the self-energy must be momentum-independent and given by the **self-consistent equation**

$$\Sigma(\omega) = \frac{\frac{1}{2} z^2 t^2}{\omega - Jz - \Sigma(\omega - Jz)}. \tag{4.71}$$

This self-energy is exactly the same as the self-energy of a single dopant moving through an **Ising antiferromagnet**.[42] In fact, in any system where a moving particle automatically excites a gapped and flat mode the self-consistent equation (4.71) applies.

[42] Kane et al., 1989

As described in Kane et al., 1989, a hole in an Ising antiferromagnet is effectively confined by the surrounding magnetic texture. Each hop away from its initial point increases the energy, thus creating a linear potential well for the hole. In such a linear confinement potential a ladder spectrum appears where the energy distance between the to lowest peaks scales as $t(J/t)^{2/3}$. The spectral weight carried by higher order peaks vanishes as $t/J \to 0$.[43]

[43] Kane et al., 1989

The Ising-like features in the exciton spectral function are explicitly visible in the numerically computed dispersions shown in figures 4.7 and 4.14. We indeed conclude that the visibility of the ladder spectrum is actually enhanced in the bilayer case presented here relative to the hole in the single layer due to the nondispersive interlayer spin excitations.

Of course the exciton ladder spectrum in figure 4.7 is not exactly sharp. By the above analysis, we can infer that the incoherent broadening of peaks is due to interactions with the transversal spin waves. Indeed, the transversal spin waves can be viewed as the equivalent of the single layer spin waves. Therefore for small α the effect of transversal spin waves is to mildly quantize the Ising limit, and the results become reminiscent of a single hole in the $t-J$ model, including the quasiparticle peak broadening.

4.2.4 *Relation to experiment*

The formation of kinetically frustrated bound exciton states can be experimentally verified by measurements of the dielectric function or any other charge-excitation measurements. One particular example is **electron energy loss spectroscopy (EELS)**, showing for instance clear signatures of the in-plane charge transfer excitons in cuprates.[44] The EELS cross-section is directly related to the **dielectric function**[45] via the dynamical structure factor $S(q,\omega)$,

[44] Wang et al., 1996; and Zhang and Ng, 1998

[45] Schnatterly, 1979

$$d\sigma \propto \frac{1}{q^4} S(q,\omega) \propto \frac{1}{q^2} \mathrm{Im}\left[\frac{-1}{\epsilon(q,\omega)}\right] \tag{4.72}$$

with the dynamical structure factor defined as

$$\begin{aligned} S(q,\omega) &= \frac{1}{N}\int \frac{dt}{2\pi} e^{-\epsilon|t|} \sum_\lambda \langle\psi_0| \sum_i e^{-iq\cdot r_i} e^{i(\omega-H)t} |\lambda\rangle \\ &\quad \times \langle\lambda| \sum_j e^{iq\cdot r_j} |\psi_0\rangle \end{aligned} \tag{4.73}$$

where the sum λ runs over all intermediate states, and $|\psi_0\rangle$ is the initial state of the system. We use the dipole expansion such that

$$e^{iqr_i} = 1 + i\vec{q}\cdot\vec{r}_i + \dots \tag{4.74}$$

where the electron position operator can be expanded in terms of the possible electron wave functions in the tight binding approximation,

$$\sum_i \vec{r}_i = \sum_{ij\sigma} c^\dagger_{i\sigma} c_{j\sigma} \langle \phi_i | \vec{r} | \phi_j \rangle \tag{4.75}$$

where $|\phi_i\rangle$ are the Wannier wave functions of the electron on site i. The z component of $\langle \phi_i | \vec{r} | \phi_j \rangle$ is proportional to the interlayer hopping energy $t_\perp$, which in turn is equal to the the creation operator of an exciton,

$$\begin{aligned} r^z &\propto t_\perp \sum_{i\sigma} c^\dagger_{in\sigma} c_{ip\sigma} + h.c. && (4.76)\\ &\propto t_\perp \sum_i \left(E^\dagger_i + E_i \right) && (4.77) \end{aligned}$$

We recognize the Fourier transform of the $k = 0$ excitonic state, so that we find

$$\begin{aligned} S(q^z, \omega) &\propto (q^z t_\perp)^2 \int \frac{dt}{2\pi} e^{-\epsilon|t|} \sum_\lambda \langle \psi_0 | E_{k=0}\, e^{i(\omega - H)t} | \lambda \rangle \\ &\quad \times \langle \lambda |\, E^\dagger_{k=0} | \psi_0 \rangle. \end{aligned} \tag{4.78}$$

We have introduced the term $e^{-\epsilon|t|}$ to ensure convergence of the integral so that we can integrate over t. We find that the dynamic structure factor is directly related to the exciton spectral function

$$\begin{aligned} S(q^z, \omega) &\propto (q^z t_\perp)^2 \langle \psi_0 | E_{k=0} \left(\frac{i}{\omega - H + i\epsilon} - \right. \\ &\quad \left. \frac{i}{\omega - H - i\epsilon} \right) E^\dagger_{k=0} | \psi_0 \rangle \\ &\propto (q^z t_\perp)^2 A(k = 0, \omega) \end{aligned} \tag{4.79}$$

or in other words

$$\mathrm{Im}\left[\epsilon^{-1}(q^z, \omega) \right] \sim (t_\perp)^2 A(k = 0, \omega). \tag{4.80}$$

Consequently, one expects the bound exciton states to show up in EELS measurements when probing the z-axis excitations. In addition to the bound exciton states, a broad electron-hole continuum will show up at high energies.

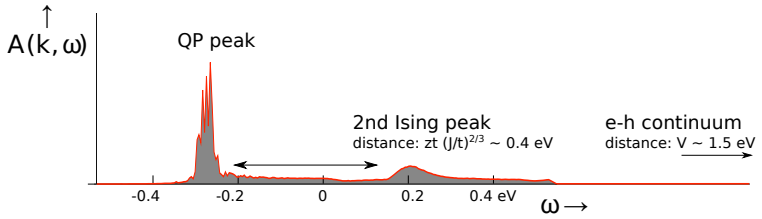

Figure 4.15: Expected zero-momentum exciton spectral function for the c-axis charge-transfer exciton in YBCO bilayers. We used model parameters $J = 0.125$ eV, $t = 0.1$ eV and $\alpha = 0.04$. A pronounced quasiparticle peak is followed at a distance of $zt(J/t)^{2/3}$ by a secondary peak as a sign of Ising confinement. The electron-hole continuum sets in at an energy $V \sim 1.5$ eV above the center of this spectrum. The momentum dependence of this spectrum is shown in figure 4.8.

Another possible way to detect interlayer excitons is to use optical probes. The **optical conductivity** $\sigma(q, \omega)$ of a material is related to the dielectric function[46] by

$$\epsilon^{-1}(q, \omega) = 1 - i\frac{q^2}{\omega} V_c(q)\sigma(q, \omega), \tag{4.81}$$

where $V_c(q)$ is the Fourier transform of the Coulomb potential $\frac{1}{\epsilon_0|r-r'|}$. The real part of the c-axis optical conductivity is therefore proportional to the exciton spectral function. Similar considerations hold when one measures the **Resonant Inelastic X-ray Scattering (RIXS)**[47] spectrum.

[46] Bruus and Flensberg, 2004

[47] Ament et al., 2011

When comparing the dielectric function with the computed spectral functions in figures 4.12-4.15, do bear in mind that the latter are shifted over an energy E_0 required to excite an interlayer exciton. This energy is of the order of electron volts. For example, along the ab-plane in cuprates charge-transfer excitons are observed in the range of 1-2 eV.[48] Since the energy required for a charge-transfer excitation is largely dependent on the onsite repulsion, we expect that the c-axis exciton will be visible at comparable energy scales.

[48] Basov and Timusk, 2005

How would then the exciton spectrum look like for a realistic material, such as the **bilayer cuprate $YBa_2Cu_3O_{7-\delta}$ (YBCO)**? Following earlier neutron scattering experiments[49] one can deduce that the effective $J = 125 \pm 5$ meV and $J_\perp = 11 \pm 2$ meV, which corresponds to an effective value of $\alpha = 0.04\alpha_c$ where α_c is the critical value of α.[50] The question remains what a realistic estimate of the exciton binding energy is. The planar excitons are known to be strongly bound[51] with binding energy of the order of 1-2 eV. Since the Coulomb repulsion scales as $V \sim (\epsilon r)^{-1}$, we can relate the binding energy of the interlayer excitons to that of the planar excitons. The distance between the layers is about twice

[49] Imada et al., 1998; and Tranquada et al., 1989

[50] Chubukov and Morr, 1995

[51] Zhang and Ng, 1998

the in-plane distance between nearest neighbor copper and oxygen atoms, but simultaneously we expect the dielectric constant ϵ_c along the c-axis to be smaller than ϵ_{ab} due to the anisotropy in the screening. Combining these two effects, we consider it a reasonable assumption that the interlayer exciton binding energy is comparable to the in-plane binding energy. The hopping energy for electrons is approximately $t_e = 0.4$ eV which yields, together with a Coulomb repulsion estimate of $V \sim 1.5$ eV, an effective exciton hopping energy of $t \sim 0.1$ eV. Note that these estimates of V/t justify our use of the strong coupling limit in section 4.1.3.

The spectral function corresponding to these parameters is shown in figure 4.15. Since $t \sim J$ the ladder spectrum is strongly suppressed compared to the aforementioned anti-adiabatic limit. However, the Ising confinement still shows its signature in a small 'second ladder peak' at 0.4 eV energy above the exciton quasiparticle peak. To the best of our knowledge and to our surprise, the c-axis optical conductivity of YBCO has not been measured before in the desired regime with energies above 1 eV.[52] Detection of this second ladder peak in future experiments would suggest that indeed the interlayer excitons in cuprates are frustrated by the spin texture.

[52] Confirmed in private communications with D. van der Marel. In addition, standard review articles on optical absorption in cuprates (such as Basov and Timusk, 2005) indeed only show infrared measurements ($< 1000\,\mathrm{cm}^{-1}$) of the c-axis optical absorption in insulating cuprates.